
Proceedings Paper:
Lesnic, D orcid.org/0000-0003-3025-2770, Altalhi, NR and Griffiths, SD (Accepted: 2023) The boundary element method for solving rigid inclusion problems. In: Proceedings of the Thirteenth UK Conference on Boundary Integral Methods (UKBIM13). 13th UK Conference on Boundary Integral Methods, 10-11 Jul 2023, Aberdeen, UK. University of Aberdeen . (In Press)

Chapter 1

The boundary element method for solving rigid inclusion problems

N.R. Altalhi[1,2], D. Lesnic[1] and S.D. Griffiths[1]

[1] Department of Applied Mathematics,
University of Leeds
Leeds LS2 9JT, UK
mmnrah@leeds.ac.uk, d.lesnic@leeds.ac.uk, s.d.griffiths@leeds.ac.uk

[2] Department of Applied Mathematics,
University of Taif
Taif, Saudi Arabia
nrtalhi@tu.edu.sa

Abstract. *Electrostatics (or steady-state temperature) probing fields in a domain containing a rigid inclusion, e.g., the domain outside an underground pipe, can be described by a Dirichlet problem for the Laplace equation in an annulus in which on the inner boundary the solution takes an unknown, but constant, value. For such a problem, the boundary element method (BEM) is well-suited. The extra unknown represented by the constant value of the electric potential on the inner boundary is determined by imposing that the integral of the current flux over the outer boundary of the annular domain vanishes. Numerical results are presented and discussed showing the convergence and accuracy of the BEM.*

1.1 Introduction

One of the most crucial engineering topic for the nuclear power plant's safety administration is corrosion in pipes [8]. Corrosion can lead to leaks, ruptures, and other forms of damage in pipes, which can cause safety hazards and costly repairs. Detecting and monitoring corrosion is, therefore, essential for ensuring the integrity of the pipes and the safety and efficiency of nuclear power plants.

Electrostatics or steady-state temperature fields can be used to detect corrosion in pipes by evaluating changes in the electric field and temperature distribution caused by corrosion-induced changes in the thermal properties of material. This requires resolving Laplace's equation in an approximately annular domain with corrosion deviations, and imposing boundary conditions on the inner and outer boundaries to estimate the electric potential or temperature distribution.

These methods involve solving the Dirichlet problem for the Laplace equation in an annular domain, where the solution takes an unknown, but constant, value on the inner boundary.

The boundary element method (BEM) has gained a great deal of study in a variety of engineering disciplines for the purpose of solving mainly linear partial differential equations (PDE) with fundamental solution available in explicit form, and significant advancements have been made in the theoretical, numerical and practical aspects. The BEM has received considerable attention from both academic research groups and the engineering community [6, 2]. The BEM remains a topic of active research, and it continues to present a range of challenging issues for theorists, numerical analysts and experimenters alike. Our numerical simulations show that the BEM can accurately determine the current flux and the electric potential on the inner boundary and inside the solution domain, providing a fast an accurate direct solver for the nonlinear minimization that is usually employed in the detection of corrosion [3, 7].

The paper is organised as follows. In Section 1.2, we formulate the mathematical problem under investigation, whilst in Section 1.3, the BEM is implemented. Section 1.4 discusses the numerically obtained results in order to demonstrate the convergence and accuracy of the BEM. Finally, conclusions are included in Section 1.5.

1.2 Mathematical formulation

Let $\Omega_1 \subset \Omega_0$ be two-dimensional simply-connected bounded domains with sufficiently smooth boundaries $\partial\Omega_1$ and $\partial\Omega_0$, e.g., of class C^2, see Fig. 1.1. The solution domain $\Omega := \Omega_0 \backslash \Omega_1$ is the doubly-connected annular domain in between $\partial\Omega_0$ and $\partial\Omega_1$. Let us assume that Ω is a body with constant conductivity (anisotropic functionally graded media are also ameneable with our BEM). In domain Ω, the electrostatic field is taken into consideration by seeking a harmonic function $u \in C^2(\Omega) \cap C^1(\overline{\Omega})$, representing the electrical potential, satisfying the Laplace's equation

$$\Delta u = 0 \qquad \text{in} \quad \Omega, \tag{1.1}$$

subject to the Dirichlet boundary conditions

$$u = f \qquad \text{on} \quad \partial\Omega_0, \tag{1.2}$$

$$u = a \qquad \text{on} \quad \partial\Omega_1, \tag{1.3}$$

where $f \in C(\partial\Omega)$ is a given Dirichlet data on the outer boundary $\partial\Omega_0$ and a is a constant. Equation (1.3) models the fact that Ω_1 is a (perfectly conducting) rigid inclusion (while noting that an adiabatic zero-Neumann boundary condition on $\partial\Omega_1$ models a cavity). If a is given, then the problem in Eqs. (1.1)-(1.3) has a unique solution u. However, if the constant a is not known then the additional condition

$$\int_{\partial\Omega_0} \frac{\partial u}{\partial n} ds = 0, \tag{1.4}$$

where n is the outward unit normal to the boundary $\partial\Omega$, ensures the uniqueness of solution (u, a) to the problem in Eqs. (1.1)-(1.4), see [3]. The BEM numerical approximations of the problem in Eqs. (1.1)-(1.3) with a known, or Eqs. (1.1)-(1.4) with a unknown, will be illustrated in Section 1.3.

In electrical impedance tomography (EIT), the obstacle Ω_1 is also unknown and in order to compensate for this missing information one measures the current flux $g \in C(\partial\Omega_0)$ given by

$$\frac{\partial u}{\partial n} = g \qquad \text{on} \quad \partial\Omega_0. \tag{1.5}$$

However, this more complex nonlinear inverse problem of EIT, [1, 3, 5], will not be investigated herein.

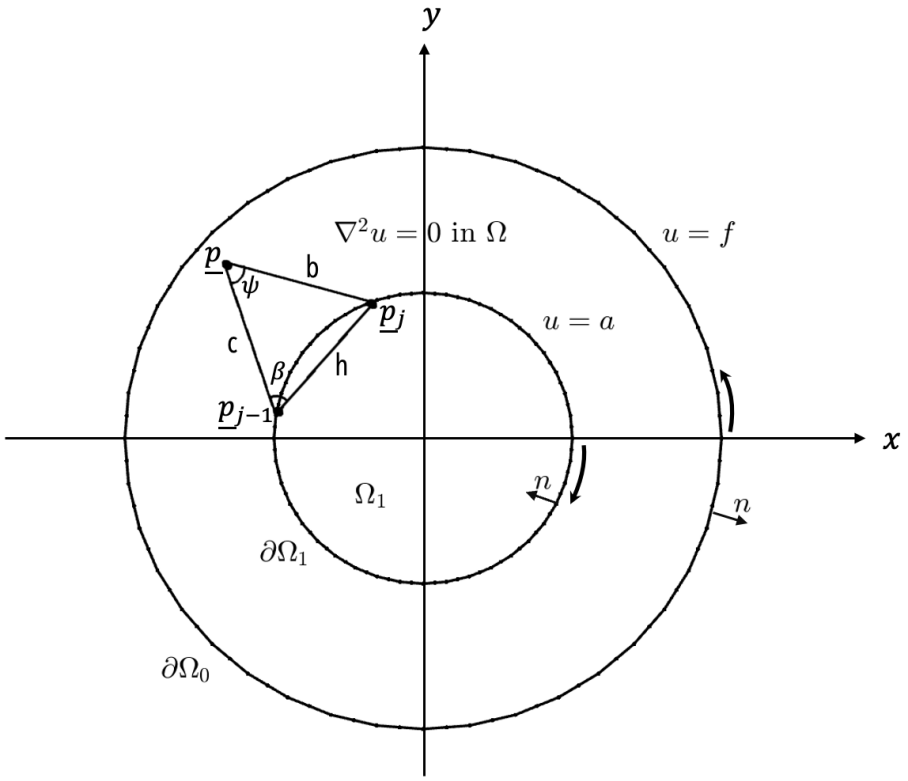

Figure 1.1: The boundary value problem in Eqs. (1.1)-(1.3) and the BEM discretisation of the boundary $\partial\Omega = \partial\Omega_0 \cup \partial\Omega_1$.

1.3 Boundary element method (BEM)

In [3], the author employed a single-layer representation of the harmonic function u that was further differentiated in the tangential and normal directions at the boundary in order to apply the conditions (1.3) and (1.4). In our study, we use a combined single-double layer classical representation, based on the Green's formula, which avoids these differentiations and enables direct applications of conditions (1.3) and (1.4).

Application of the BEM to Laplace's equation (1.1) in two-dimensions, [7], results in

$$\eta(\underline{p})u(\underline{p}) = \int_{\partial\Omega} \Big[G(\underline{p},\underline{p}')\frac{\partial u}{\partial n}(\underline{p}') - u(\underline{p}')\frac{\partial G}{\partial n(\underline{p}')}(\underline{p},\underline{p}') \Big] ds(\underline{p}'), \quad \underline{p} \in \overline{\Omega}, \tag{1.6}$$

where $\eta(\underline{p}) = 1$ if $\underline{p} \in \Omega$ and $\eta(\underline{p}) = 1/2$ if $\underline{p} \in \partial\Omega$ (smooth), and G is the fundamental solution of the Laplace equation, which, in two-dimensions, is given by

$$G(\underline{p}, \underline{p}') = -\frac{1}{2\pi} \ln |\underline{p} - \underline{p}'|. \tag{1.7}$$

Applying Eq. (1.6) at $\underline{p} \in \partial\Omega = \partial\Omega_0 \cup \partial\Omega_1$ and using the boundary conditions (1.2) and (1.3) result in

$$\int_{\partial\Omega} G(\underline{p}, \underline{p}') \frac{\partial u}{\partial n}(\underline{p}') ds(\underline{p}') - \int_{\partial\Omega_0} f(\underline{p}') \frac{\partial G}{\partial n(\underline{p}')}(\underline{p}, \underline{p}') ds(\underline{p}') - a \int_{\partial\Omega_1} \frac{\partial G}{\partial n(\underline{p}')}(\underline{p}, \underline{p}') ds(\underline{p}') = \begin{cases} \frac{1}{2} f(\underline{p}) & \text{if } \underline{p} \in \partial\Omega_0, \\ \frac{1}{2} a & \text{if } \underline{p} \in \partial\Omega_1. \end{cases} \tag{1.8}$$

We discretise the boundary $\partial\Omega = \partial\Omega_0 \cup \partial\Omega_1$ of the solution domain $\Omega = \Omega_0 \backslash \Omega_1$ into a series of $M = 2N$ boundary elements. The outer boundary $\partial\Omega_0$ is discretised anti-clockwise into a series of N straight line segments $\Gamma_j^0 = [\underline{p}_{j-1}, \underline{p}_j]$ for $j = \overline{1, N}$, where $\underline{p}_N = \underline{p}_0$, while the inner boundary $\partial\Omega_1$ is discretised clockwise into a series of N straight line segments $\Gamma_{j-N}^1 = [\underline{p}_j, \underline{p}_{j+1}]$ for $j = \overline{N+1, 2N}$, where $\underline{p}_{2N+1} = \underline{p}_{N+1}$. Let as denote

$$\Gamma_j = \begin{cases} \Gamma_j^0 & \text{for } j = \overline{1, N}, \\ \Gamma_j^1 & \text{for } j = \overline{N+1, 2N}. \end{cases}$$

Over each small boundary element Γ_j, the unknown Neumann data $\partial u/\partial n$ is assumed constant and take the value at the midpoint (boundary element node)

$$\tilde{\underline{p}}_j = \begin{cases} (\underline{p}_j + \underline{p}_{j-1})/2 & \text{for } j = \overline{1, N}, \\ (\underline{p}_{j+1} + \underline{p}_j)/2 & \text{for } j = \overline{N+1, 2N}, \end{cases}$$

namely

$$\frac{\partial u}{\partial n}(\underline{p}) \approx \frac{\partial u}{\partial n}(\tilde{\underline{p}}_j) =: u_j' \qquad \text{for} \quad \underline{p} \in \Gamma_j, \quad j = \overline{1, 2N}. \tag{1.9}$$

We also approximate the Dirichlet data f in Eq. (1.2) by a piece-wise constant function as

$$f(\underline{p}) \approx f(\tilde{\underline{p}}_j) =: f_j \qquad \text{for} \quad \underline{p} \in \Gamma_j^0, \quad j = \overline{1, N}. \tag{1.10}$$

Denote

$$A_j(\underline{p}) := \int_{\Gamma_j} G(\underline{p}, \underline{p}') ds(\underline{p}'), \quad B_j(\underline{p}) := \int_{\Gamma_j} \frac{\partial G}{\partial n(\underline{p}')}(\underline{p}, \underline{p}') ds(\underline{p}'), \quad \underline{p} \in \overline{\Omega}, \quad j = \overline{1, 2N}. \tag{1.11}$$

With the approximations Eqs. (1.9) and (1.10), the boundary integral equation (1.8) is approximated as

$$\sum_{j=1}^{2N} A_j(\underline{p}) u_j' - \sum_{j=1}^{N} B_j(\underline{p}) f_j - a \sum_{j=N+1}^{2N} B_j(\underline{p}) = \begin{cases} \frac{1}{2} f(\underline{p}) & \text{if } \underline{p} \in \partial\Omega_0, \\ \frac{1}{2} a & \text{if } \underline{p} \in \partial\Omega_1. \end{cases} \tag{1.12}$$

The approximation of the boundary by straight line segments enables us to evaluate the integrals $A_j(\underline{p})$ and $B_j(\underline{p})$ in Eq. (1.11) analytically for every $\underline{p} \in \overline{\Omega}$ and their expressions are given by

$$A_j(\underline{p}) = A(\underline{p}, \underline{p}_{j-1}, \underline{p}_j) = -\frac{1}{2\pi} \begin{cases} h(\ln(h) - 1) & \text{if } cb = 0, \\ c\cos(\beta)\ln(c/b) - h(1 - \ln(b)) + c\,\psi\sin(\beta) & \text{if } cb \neq 0, \end{cases} \tag{1.13}$$

$$B_j(\underline{p}) = B(\underline{p}, \underline{p}_{j-1}, \underline{p}_j) = \frac{1}{2\pi} \begin{cases} 0 & \text{if } cb = 0 \text{ or } \underline{p} \in \overline{\underline{p}_{j-1}, \underline{p}_j}, \\ \psi\ \text{sign}(\alpha_{j-1}(\underline{p}) - \alpha_j(\underline{p})) & \text{if } y \in [y_{j-1}, y_j], \\ \psi\ \text{sign}(\alpha_j(\underline{p}) - \alpha_{j-1}(\underline{p})) & \text{otherwise}, \end{cases} \tag{1.14}$$

where sign is the signum function, defined by

$$\text{sign}(x) = \begin{cases} -1 & \text{if } x < 0, \\ 0 & \text{if } x = 0, \\ 1 & \text{if } x > 0, \end{cases}$$

and, see Figure 1.1, $c = |\underline{p} - \underline{p}_{j-1}|$, $b = |\underline{p} - \underline{p}_j|$, $h = |\underline{p}_j - \underline{p}_{j-1}|$, $\alpha_{j-1}(\underline{p}) \in [0, \pi]$ and $\alpha_j(\underline{p}) \in [0, \pi]$ are the angles between the positive x-axis and the straight lines $\overline{\underline{p}\underline{p}_{j-1}}$ and $\overline{\underline{p}\underline{p}_j}$ in the upper half plane, respectively, and the angles $\psi \in [0, \pi]$ and $\beta \in [0, \pi]$ are given by

$$\psi = \arccos\left(\frac{c^2 + b^2 - h^2}{2cb}\right), \quad \beta = \arccos\left(\frac{c^2 + h^2 - b^2}{2ch}\right). \tag{1.15}$$

Collocating Eq. (1.12) at $\underline{p} = \underline{\tilde{p}}_i$ for $i = \overline{1, 2N}$, we obtain

$$\sum_{j=1}^{2N} A_{ij} u'_j + \sum_{j=1}^{2N} B_{ij} f_j = 0, \qquad i = \overline{1, 2N}. \tag{1.16}$$

where

$$\begin{aligned} &A_{ij} := A_j(\underline{\tilde{p}}_i), \quad B_{ij} := -\frac{1}{2}\delta_{ij} - B_j(\underline{\tilde{p}}_i), \quad i, j = \overline{1, 2N}, \\ &f_j = f(\underline{\tilde{p}}_j), \quad j = \overline{1, N} \quad \text{and} \quad f_j = a, \quad j = \overline{N+1, 2N}, \end{aligned} \tag{1.17}$$

and $\delta_{i,j}$ the Kronecker delta symbol.

In the case a is known, the system of equations (1.16) can be written in compact form as

$$A\underline{u'} = -B\underline{f} \tag{1.18}$$

and solved using the Matlab command of the LU decomposition method.

In the case a is unknown, the system of equations (1.16) can be written in the form

$$\sum_{j=1}^{2N} A_{ij} u'_j + a \sum_{j=N+1}^{2N} B_{ij} = -\sum_{j=1}^{N} B_{ij} f_j, \qquad i = \overline{1, 2N}, \tag{1.19}$$

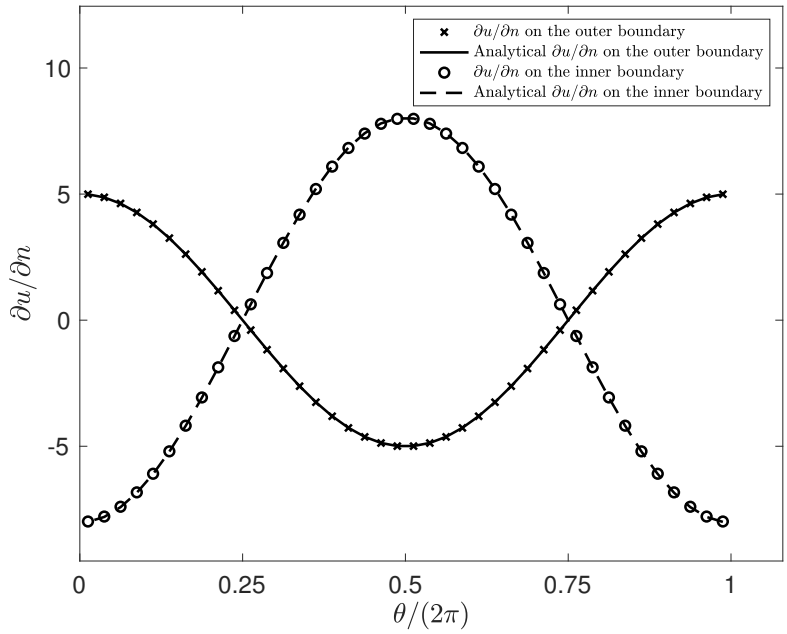

Figure 1.2: The analytical (1.25) and numerical normal derivatives on the outer and inner boundaries, as functions of $\theta/(2\pi)$, obtained using the BEM with $N = 40$, for the problem given by Eqs.(1.1), (1.22) and (1.23).

Equation (1.4) is also employed in the discretized form,

$$\sum_{j=1}^{N} h_j u'_j = 0, \tag{1.20}$$

where $h_j := \int_{\Gamma_j} ds(\underline{p}')$ for $j = \overline{1, N}$.

The new system of linear equations (1.19) and (1.20) is solved using the Matlab command of the LU decomposition method to find the Neumann values $u'_{j=\overline{1,2N}}$ and the constant a.

Once the values of $\underline{u}'$ (and a when unknown) have been found accurately, the following discretisation of the integral Eq. 1.12:

$$u(\underline{p}) = \sum_{j=1}^{2N} A_j(\underline{p}) u'_j - \sum_{j=1}^{N} B_j(\underline{p}) f_j - a \sum_{j=N+1}^{2N} B_j(\underline{p}), \quad \underline{p} \in \Omega, \tag{1.21}$$

provides explicitly the solution $u(\underline{p})$ at any point $\underline{p}$ inside the solution domain Ω.

1.4 Numerical results and discussion

Let Ω_0 and Ω_1 be the discs of radii R_0 and R_1, where $0 < R_1 = 0.5 < R_0 = 1$ centered at the origin, as shown in Figure 1.1.

	u_N				u_{exact}
	$N = 10$	$N = 20$	$N = 40$	$N = 80$	
$u(0.8, 0.0)$	1.8793	1.9363	1.9467	1.9491	1.9500
$u(0.6, 0.3)$	1.0296	1.0568	1.064	1.0660	1.0666
$u(-0.3, 0.6)$	-0.5179	-0.5284	-0.5320	-0.5330	-0.5333

Table 1.1: The exact (1.24) and numerical BEM solutions obtained with various numbers of boundary elements $N \in \{10, 20, 40, 80\}$, for the problem given by Eqs. (1.1), (1.22) and (1.23).

1.4.1 Example when a is known

With the boundary conditions (1.2) and (1.3) given by

$$u(r,\theta)|_{r=R_0=1} = f(R_0,\theta) = 3\cos(\theta) \qquad \text{on} \quad \partial\Omega_0, \tag{1.22}$$

$$u(r,\theta)|_{r=R_1=0.5} = a = 0 \qquad \text{on} \quad \partial\Omega_1, \tag{1.23}$$

it is easy to see that the problem in Eqs. (1.1), (1.22) and (1.23) has the analytical solution

$$u(r,\theta) = 4r\cos(\theta) - \frac{\cos(\theta)}{r}, \quad R_1 < r < R_0, \quad r \in [0, 2\pi). \tag{1.24}$$

From (1.24), the exact current flux is given by

$$\left.\frac{\partial u}{\partial n}\right|_{r=R_0} = 4\cos(\theta) + \frac{\cos(\theta)}{R_0^2}, \quad \left.\frac{\partial u}{\partial n}\right|_{r=R_1} = -\left(4\cos(\theta) + \frac{\cos(\theta)}{R_1^2}\right), \quad \theta \in [0, 2\pi). \tag{1.25}$$

As shown in Figure 1.2, the agreement between the BEM numerical solution and the exact solution for the normal derivative is excellent.

In order to choose the right number of boundary elements for a specific problem, it is crucial to know how fast the numerical solution reaches the true solution, as the number of boundary elements increases. In Table 1.1, the number of boundary elements used determines the accuracy of the numerical solution obtained using the BEM. For instance, at $(-0.3, 0.6)$, the numerical solution becomes more accurate since the absolute error $\{0.0153, 0.0049, 0.0012, 0.0003\}$ decreases as the number of boundary elements increases from $N = 10$ to 20, 40 and 80, as shown in Table 1.1. The solutions become more accurate as more boundary elements are used.

It is illustrative to examine the convergence behaviour of the BEM using a plot, see Figure 1.3(a), and calculate order of convergence of the BEM. The computational order of convergence is defined as [4],

$$\alpha \approx \frac{\ln\left(\frac{e_{new}}{e_{old}}\right)}{\ln\left(\frac{N_{new}}{N_{old}}\right)}, \tag{1.26}$$

where e_{new} and e_{old} denote the absolute errors of the numerical solutions obtained with N_{new} and N_{old} boundary elements, respectively. For our problem we have calculated the order of convergence for $u(0.8, 0.0)$ and obtained $\alpha \in \{2.3699, 2.0625, 1.9965\}$ for $\{10, 20, 40\} \ni N_{old} = N_{new}/2$, see Figure 1.3(a). This indicates that the order of convergence is quadratic.

The L^2-norm of error gives a measure of the overall accuracy of the numerical approximation, see Figure 1.3(b). To compute the L^2-norm numerically, we use a Gaussian quadrature technique over a triangulated mesh that covers the domain Ω using the PDE Toolbox in Matlab. The sum of the approximations over all mesh elements yields the L^2-norm squared of the error. The formula for the L^2-norm of a function $U(x, y)$ over a domain Ω is

$$||U||_{L^2(\Omega)} = \left(\int_\Omega U^2(x, y) dx dy \right)^{1/2}. \tag{1.27}$$

By using Eq. (1.26), the estimated values of α of $\{4.7044, 1.8012, 2.1346\}$ for $\{10, 20, 40\} \ni N_{old} = N_{new}/2$ are obtained for the $L^2(\Omega)$ errors presented in Figure 1.3(b), indicating the quadratic order of convergence.

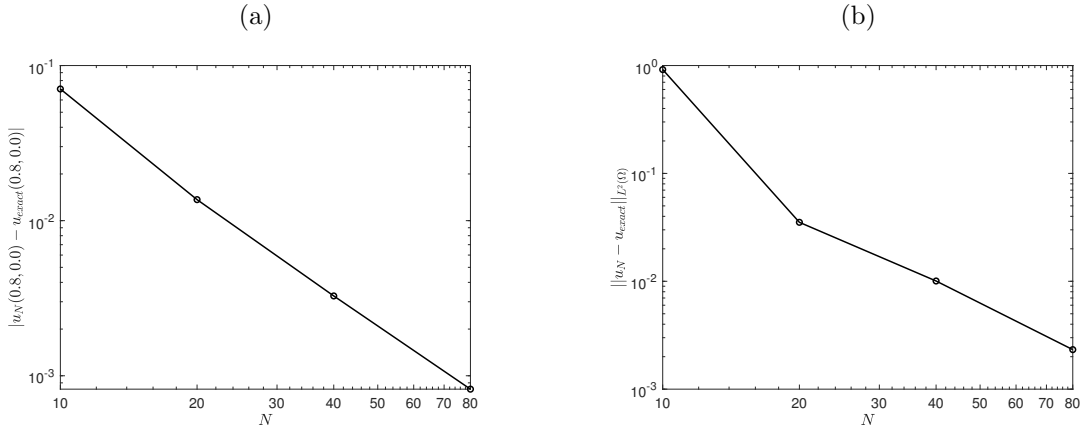

Figure 1.3: The convergence of the BEM at (a) the point $(0.8, 0.0)$ and (b) in $L^2(\Omega)$ for the problem given by Eqs. (1.1), (1.22) and (1.23).

1.4.2 Example when a is unknown

Consider now the same problem given by equations (1.1), (1.3) and (1.22) in the annular domain $\Omega = \{(r, \theta)\} |\ 0.5 = R_1 < r < R_0 = 1,\ \theta \in [0, 2\pi)\}$, but now the constant a is unknown. Then, equations (1.19) and (1.20) can be written as the linear system of algebraic equations

$$\tilde{A} \begin{pmatrix} \underline{u}' = (u'_j)_{j=\overline{1,2N}} \\ a \end{pmatrix} = \underline{C}, \tag{1.28}$$

where the matrix $\tilde{A}$ is given by

$$\tilde{A}_{ij} = \begin{cases} A_{ij} & \text{if } \ i = \overline{1, 2N}, j = \overline{1, 2N} \\ h_j & \text{if } \ i = 2N + 1, j = \overline{1, N} \\ 0 & \text{if } \ i = 2N + 1, j = \overline{N + 1, 2N + 1} \\ 0 & \text{if } \ i = \overline{1, N}, j = 2N + 1 \\ -1 & \text{if } \ i = \overline{N + 1, 2N}, j = 2N + 1, \end{cases}$$

and

$$\underline{C} = (C_i)_{i=\overline{1,2N+1}} \text{ with } C_i = -\sum_{j=1}^{N} B_{ij} f_j \text{ for } i = \overline{1,2N} \text{ and } C_{2N+1} = 0.$$

Table 1.2 shows the numerical BEM solutions at the points: $(0.8, 0.0), (0.6, 0.3)$, and $(-0.3, 0.6)$

	u_N				u_{exact}
	$N = 10$	$N = 20$	$N = 40$	$N = 80$	
$u(0.8, 0.0)$	1.9281	1.9504	1.9503	1.9501	1.9500
$u(0.6, 0.3)$	1.1169	1.0803	1.0701	1.0675	1.0666
$u(-0.3, 0.6)$	-0.5623	-0.5401	-0.5350	-0.5337	-0.5333
a	-4.7E-15	5.6E-14	-3.9E-13	-1.0E-12	0

Table 1.2: The exact (1.24) and numerical BEM solutions obtained with various numbers of boundary elements $N \in \{10, 20, 40, 80\}$ for the problem given by Eqs. (1.1), (1.3), (1.4) and (1.22).

converging to the exact solution (1.24). The numerically retrieved values of the constant a are also close to the exact value of zero. The estimated values of $\alpha \in \{4.6420, 1.8231, 2.1155\}$ for $\{10, 20, 40\} \ni N_{old} = N_{new}/2$ are obtained for the $L^2(\Omega)$ errors, indicating the quadratic order of convergence. These values are similar to those obtained for the problem of the previous section 1.4.1 where a was known.

We consider now an example in which an analytical solution is not available. Here we take the Dirichlet data (1.2) given by, [3],

$$u(r,\theta)|_{r=R_0=1} = f(R_0,\theta) = 10\left(\exp\left[-4\sin^2(\theta/2)\right] - \exp\left[-4\cos^2(\theta/2)\right]\right), \quad \theta \in [0, 2\pi). \quad (1.29)$$

The numerical results presented in Table 1.3 show the convergence of the BEM numerical solution.

	u_N			
	$N = 10$	$N = 20$	$N = 40$	$N = 80$
$u(0.8, 0.0)$	6.5303	6.2997	6.2097	6.1858
$u(0.6, 0.3)$	3.5701	3.2147	3.1353	3.1157
$u(-0.3, 0.6)$	-1.4536	-1.2937	-1.2592	-1.2507
a	-1.4E-15	1.2E-13	-1.2E-12	-4.4E-12

Table 1.3: The numerical BEM solutions obtained with various numbers of boundary elements $N \in \{10, 20, 40, 80\}$ for the problem given by Eqs. (1.1), (1.3), (1.4) and (1.29).

1.5 Conclusions

The BEM has been applied to solving the Dirichlet problem for the Laplace equation in an annular domain in case the inner core represents a rigid inclusion. The constant value a of the potential on the boundary of this perfectly conducting hole may be known or unknown. In case

a is unknown, an extra condition that the integral of the current flux vanishes over the outer boundary of the solution domain has been enforced. Numerical results have been presented and discussed showing that the BEM is convergent as the number of boundary elements increases and that the convergence is of quadratic order.

Future work will consist of solving the inverse problem in case the inner core, representing, for example, a tumour, is unknown.

Acknowledgement

N.R. Altalhi would like to thank the Leeds and Taif universities for supporting her PhD research studies at the University of Leeds. No data are associated with this article. For the purpose of open access, the authors have applied a Creative Commons Attribution (CC BY) license to any Author Accepted Manuscript version arising from this submission.

References

[1] Borman, D., Ingham, D.B., Johansson, B.T. and Lesnic, D. The method of fundamental solutions for detection of cavities in EIT. *Journal of Integral Equations and Applications*, 21(3): 381-404, 2009.

[2] C. A. Brebbia, C.A., J. C. F. Telles, J,C.F. and Wrobel, L.C. *Boundary Element Techniques: Theory and Applications in Engineering*. Springer Science & Business Media, Berlin, 2012.

[3] Gavrilov, S.V. Numerical method for solving an inverse problem for Laplace's equation in a domain with an unknown inner boundary. *Computational Mathematics and Mathematical Physics*, 59(1): 59–65, 2019.

[4] Grau-Sánchez, M., Noguera, M. and Gutiérrez, J.M. On some computational orders of convergence. *Applied Mathematics Letters*, 23(4): 472–478, 2010.

[5] Karageorghis, A., Lesnic, D. and Marin, L. (2023) An efficient moving pseudo-boundary MFS for void detection. *Engineering Analysis with Boundary Elements*, 147: 90–111, 2023.

[6] Katsikadelis, J.T. *Boundary Elements: Theory and Applications.* Elsevier, Amesterdam, 2002.

[7] D. Lesnic, D., Berger, J.R. and Martin, P.A. A boundary element regularization method for the boundary determination in potential corrosion damage. *Inverse Problems in Engineering*, 10(2): 163–182, 2002.

[8] Yang, X., Choulli, M. and Cheng, J. An iterative BEM for the inverse problem of detecting corrosion in a pipe. *Numerical Mathematics*, 14(3): 252-268, 2005.